

# Performance of Water-based Liquid Scintillator

D. Beznosko<sup>c</sup>, M.V. Diwan<sup>a</sup>, S.Hans<sup>b</sup>, D. Jaffe<sup>a</sup>, S.H. Kettell<sup>a</sup>, R.Rosero<sup>b</sup>,  
H. Themann<sup>a</sup>, B. Viren<sup>a</sup>, E. Worcester<sup>a</sup>, M. Yeh<sup>b</sup>, C. Zhang<sup>a</sup>

<sup>a</sup>*Physics Department, Brookhaven National Laboratory, Upton, NY 11973, USA*

<sup>b</sup>*Chemistry Department, Brookhaven National Laboratory, Upton, NY 11973, USA*

<sup>c</sup>*Department of Physics, Nazarbayev University, Astana, 010000, KZ*

---

## Abstract

The Water-based Liquid Scintillator (WbLS) is a new material currently under development. It is based on the idea of dissolving the organic scintillator in water using special surfactants. This material strives to achieve the novel detection techniques by combining the Cerenkov rings and scintillation light, as well as the total cost reduction compared to pure liquid scintillator (LS).

Presented are the light yield measurements for the three different proton beam energies (210MeV, 475MeV and 2000MeV) for water, two different WbLS formulations (0.4% and 0.99%) and pure LS. The results show that a goal of 100 optical photons/MeV, indicated by the simulation to be an optimal light yield for observing both the Cerenkov ring and scintillation light from the proton decay in a large water detector, has been achieved.

*Keywords:* Water based, liquid scintillator, beam test

---

## 1. Motivation

In large water detectors, the Cerenkov radiation produced by a charged particle above the threshold can be used for particle identification, and the reconstruction of its direction and energy [1]. However, all charged particles below the Cerenkov threshold are missed. Detecting these below-threshold particles is important for various applications. For example, in the search of the proton decay, in the  $p^+ \rightarrow K^+ \bar{\nu}$  channel, where  $K^+$  is mostly below Cerenkov threshold and is invisible in a water detector. The use of the WbLS

---

*Email address:* `dima@dozory.us` (D. Beznosko)

9 makes the kaon visible and allows for the separation of  $K^+$ ,  $\mu^+$  and  $e^+$  signals  
10 using timing and reduce background for this decay channel.

11 In either LS or WbLS, the isotropic scintillation light is produced by  
12 the charged particle energy deposition via ionization, but the scintillator  
13 components may interfere with the Cerenkov ring detection. To detect  $K^+$   
14 and preserve the Cerenkov ring, MC studies indicate that the light yield  
15 (LY) from the scintillator component in the WbLS should be 100 optical  
16 photons/MeV.

17 Thus, WbLS potentially combines both the Cerenkov ring and scintil-  
18 lation light capabilities. It can preserve the particle identification for the  
19 particles above the Cerenkov threshold, and detect the charged particles be-  
20 low the threshold via the scintillation light. In addition, WbLS features the  
21 lower cost than pure LS and it is safer to handle[ask Minfang for reference].

22 The ability to reach the desired LY can be checked using the mono-  
23 energetic proton beam with different WbLS concentrations. For the test,  
24 the two different WbLS formulations (0.4% and 0.99%), pure water and pure  
25 LS samples were chosen. Three different proton beam energies were used  
26 with each sample. The choice of the energies comes from the following con-  
27 siderations:

- 28 • 2000MeV protons behave as minimum ionizing particle (MIP)
- 29 • 475MeV protons are just below the Cerenkov limit in water
- 30 • 210MeV protons have  $\sim$ same energy deposition as  $K^+$  from the proton  
31 decay channel mentioned above.

## 32 2. Experimental Setup

33 The experimental setup used for the proton beam test is shown in Fig-  
34 ure 1. Two tubs with the samples were used (T1 and T2). Three 2cm x  
35 2cm 5mm thick plastic scintillator hodoscopes were used (H1 to H3) with  
36 the beam trigger being formed by the coincidence of the H1&H2 only. H3  
37 was intended to verify whether particles exit T2. .

### 38 2.1. Tub and Signal Readout Description

39 Two tubs were used in the experiment:

- 40 • T1 from Polytetrafluoroethylene (PTFE) (white, highly reflective),

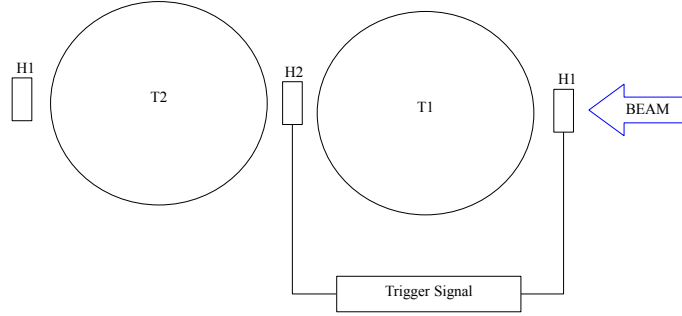


Figure 1: Proton beam test experimental setup.

- T2 from Aluminum, coated with black PTFE (very low reflectivity).

The T1 allows the capture of most of the light produced in the tub, whereas T2 allows for the observation of the light coming directly from the scintillation without the multiple wall reflections. An image of a tub is in Figure 3. Both T1 and T2 have the same dimensions:

- the lid is 19.05mm thick,
- the walls and bottom are 6.35mm thick,
- inner height and diameter are 150mm.

. A detailed setup readout scheme is shown in Figure 2. Both tubs were read out by Hamamatsu [2] R7723 2" Photo-multiplier tubes (PMT). An acrylic window transparent for the ultraviolet light (UVT) was used as a partition between the PMT and the liquid in the tub. The window was protruding through the lid and into the liquid by several millimeters to ensure that there are no air bubbles on its surface.

A readout was by the 4-channel 14bit CAEN [3] V1729A Flash Analog-to-Digital Converter (FADC). All tubs signals were connected to the FADC via a

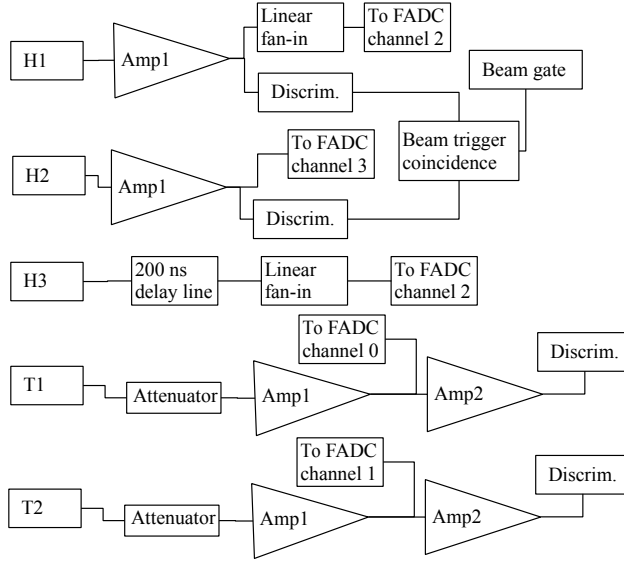


Figure 2: Proton beam test experimental setup.

variable attenuation unit (Phillips Scientific [4] 804) and a variable amplifier unit (Phillips Scientific 778). For the T1 and the T2 readouts, the gain was set to the values of  $\sim 2x$ . The first output from the amplifier goes to the FADC, with a dedicated channel for each tub. The second output from each amplifier channel was used for the single photo-electron (PE) calibration. The gain for the second amplification stage was set at  $\sim 10x$ .

All hodoscopes also were connected via  $\sim 2x$  gain amplifier channels that allows signal splitting. H1 and H3 shares the same FADC channel with latter signal being delayed by 200ns. H2 was connected to the last remaining channel of the FADC.

## 2.2. Triggering Scheme

Triggering schema was realized using three 2cm x 2cm, 5mm thick plastic scintillator counters that were readout by 2" PMTs via an air waveguide in order to remove the PMTs from direct beam exposure. The signal from the front-most and a middle counters were used to form a beam trigger, as indicated in the Figure 2.

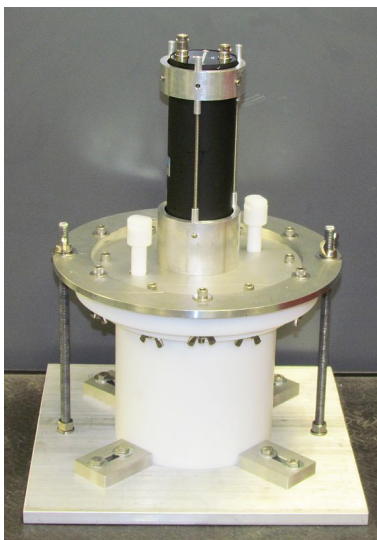


Figure 3: PTFE tub detector with a PMT.

### 74 2.3. Proton Beamline Description

75 A proton test beam was conducted at NASA Space Radiation Laboratory  
 76 (NSRL) facility at BNL. As described above, the three proton beam energies  
 77 were used: 210MeV, 475MeV and 2GeV. The beam had the following main  
 78 characteristics:

- 79 • intensity of  $\sim 1p^+$ /bunch,
- 80 • beam size was 1cm x1cm at 2GeV and 5.4cm x 5.4cm at 210MeV,
- 81 • 0.4s long spills every  $\sim 4$  sec.

## 82 3. Data Analysis

### 83 3.1. Liquids Measured

84 ???? how much details? this is a question to chemists. 4 samples tested:

- 85 • Water (purified)
- 86 • WbLS-1: 0.4%LS
- 87 • WbLS-2: 0.99%LS

- 88     • LS: 100% LS
- 89     • OR
- 90     • Water (purified)
- 91     • WbLS-1: 0.4%PC +0.4g/L PPO+3mg/L MSB+surfactant in water
- 92     • WbLS-2: 0.99%PC +1.36g/L PPO+7.48mg/L MSB+surfactant in wa-
- 93       ter
- 94     • LS: LAB + 2g/L PPO + 15mg/L MSB.

### 95   3.2. *Waveform Analysis*

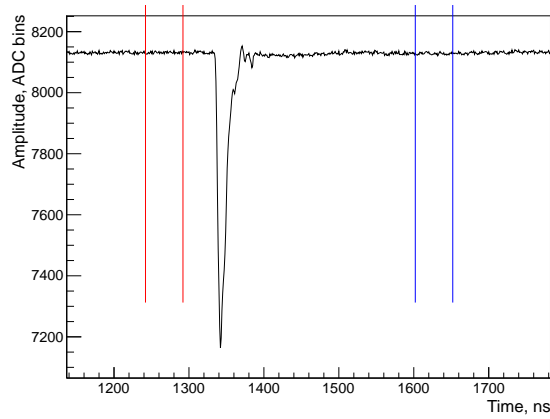


Figure 4: Typical PMT waveform with baseline check windows.

96     The PMT signal is acquired as a waveform shown in Figure 4. Total  
 97     acquisition window is 2560 bins per event with each bin being 1ns wide;  
 98     the signal is approximately centered and the approximate position is known  
 99     beforehand. A 300ns window (central one in the figure, between the red and  
 100    blue lines) is used to obtain the integrated signal area by summation. Each  
 101    point is subtracted from the average baseline to achieve a positive sum. A  
 102    typical signal is smaller then the chosen window width, however, there is a  
 103    small spread in timing of the signals and we want' to be sure that all of the  
 104    signal has been integrated. The size of the chosen window is the same for all  
 105    samples and measurements.

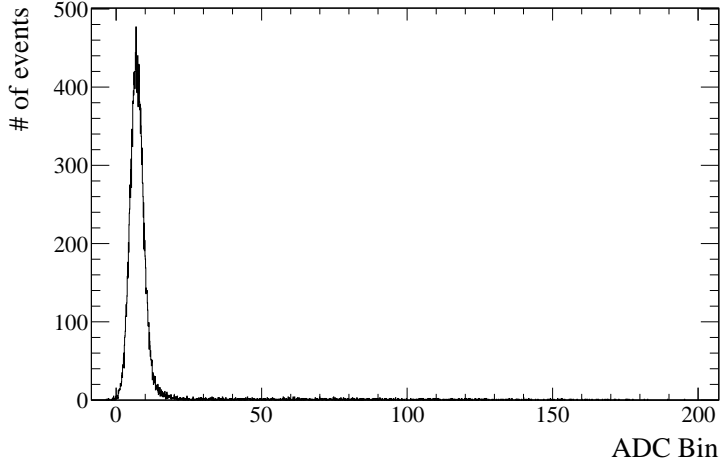


Figure 5: Typical baseline value for a single channel.

106 A baseline is defined as the average value of all the points in the first  
 107 integration window (between the two red lines) that is 50ns wide. A typical  
 108 baseline is shown in Figure 5 To check the baseline quality, its averaged value  
 109 is compared against the average of the post-signal window (between two blue  
 110 lines). This difference is illustrated in Figure 6. Events with this difference  
 111 larger then  $\sim 20$  ADC bins are flagged as bad. This allows for the removal of  
 112 the noise events or events with the bad baseline. Additionally, a comparison  
 113 of the baseline with an average of a window at the very beginning of the  
 114 waveform (between 10ns and 40ns, not shown because the figure is zoomed  
 115 around the signal area) is used for general baseline quality check using the  
 116 above criterion.

117 The integrated area is a measure of total charge that can be converted  
 118 to the PE yield using the single PE calibration of the PMTs. This allows  
 119 to describe the measured signals independent of the hardware differences  
 120 between the channels.

121 The trigger information that is saved in the two additional FADC channels  
 122 allows for the offline trigger requirements be used.

### 123 *3.3. Single Photo Electron Calibration*

124 A single PE calibration was conducted for both signal channels at the end  
 125 of the test beam run. For it, the trigger is produced from the discriminator  
 126 that follows the second amplifier for the T1 and T2 signals (separately for

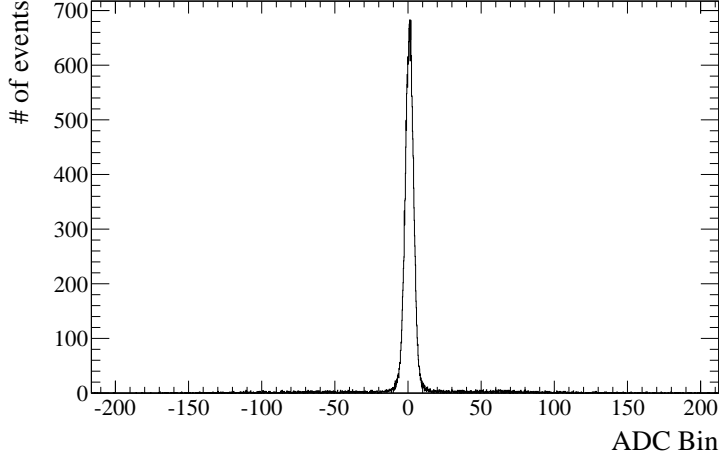


Figure 6: Difference between the baseline and the average of the post-signal window.

each, see Figure 2). The discriminator is set to  $\sim 1/10^{\text{th}}$  of the single PE amplitude as to allows for better PE signal detection efficiency than using random trigger. Additionally, this forces the PE signal to the signal window region of the FADC output for the simplified analysis and elimination of the partially captured signals. Note that a PE signal is much narrower and lower in amplitude/area then the beam signals that are typically many PEs that arrive with time distribution, thus a smaller integration window is used to reduce noise for cleaner calibration (50ns instead of 300ns).

The signal area calibration is  $168.0 \pm 1.2$  ADC bins and  $132.9 \pm 1.6$  ADC bins for T1 and T2 respectively (the PE signal is summed within the window, so the unit of ADC bin is still used). A special care was taken to separately verify that this method yields the same calibration values as using the light-emitting diode (LED) scheme. For that, calibration runs using the described above scheme and using the dim LED pulses were compared to each other. The LED light level is chosen such that only  $\sim 1/10^{\text{th}}$  of the events has the single PE signal to insure that these are the single photon detection responses.

#### 3.4. Data quality selection

The data quality selection is done as a single step before the data is analyzed. The care was taken to choose the criteria that do not introduce a bias into the selection. These are:



- offline double trigger requirement for H1 and H2 to be above  $\sim 50\text{mV}$  and within the expected time window,
- baseline quality check as outlines in chapter 3.2,
- ADC saturation check for H1 and H2.

Each check is intended to remove potential noise or multiple particles in an event. The saturation check indicates if several particles have passed through the hodoscopes in a same beam spill that happens rarely at the intensity used.

### 3.5. Light Yield Results

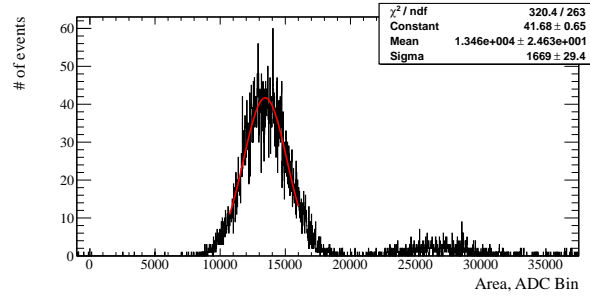


Figure 7: A sample fit of a tub signal.

For each sample and energy, a histogram of the signal areas is computed. A fit using a Gaussian and a bin likelihood method is then performed. The fitting is done in two steps - first, a Gaussian is fitted in the range between the half of the maximum peak values to obtain the first approximation. Then, the fits around the found mean with 1, 1.5 and  $2\sigma$  are carried. This is done to estimate the uncertainty that the fit width is adding because of the second peak due to the two particles passing through the tub during the same trigger time. Figure 7 shows the  $1.5\sigma$  fit of the single particle fit, and the two-particle peak is visible on it as well. This plot is in the ADC bins for clarity; single-PE calibration will be applied to all further plots.

The data for all the samples at all energies is then processed in the same way. Plots in Figure 8 and in Figure 9 show the light yield results in PE for the different samples and beam energies for Tub1 and tub2 respectively. Note that the LS light yield values plotted are reduced by a factor of 30.

170 In addition, the data point for the LS at 210MeV for T1 is not going to be  
 171 shown on further plots because of the readout saturation due to large light  
 172 amount. Similarly, the water data is not shown for T2 due to very low signal  
 173 for proton energies below the Cerenkov limit and some technical difficulties  
 174 during the data acquisition.

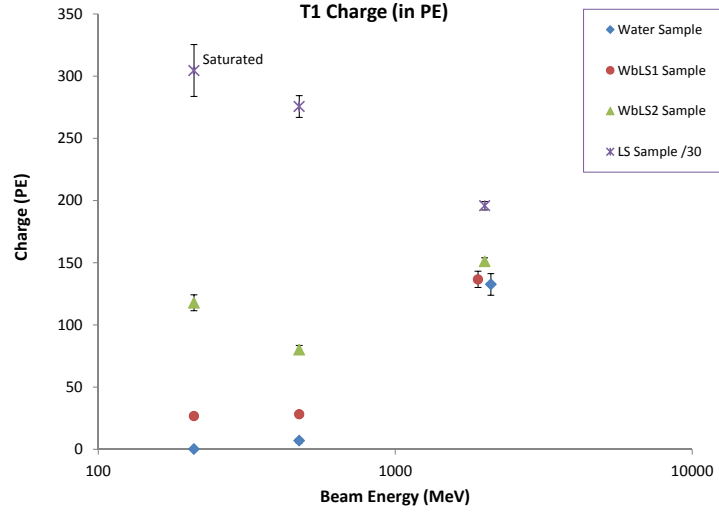


Figure 8: The light yield in PE for T1. At 2GeV beam energy, some points are offset for clarity.

### 175 3.6. Energy deposition

176 In order to assess the PE/MeV light yield of each sample, the energy  
 177 deposition in each sample is needed. Two methods were used for this purpose:  
 178 a GEANT4 simulation of the beamline setup with the deposition being the  
 179 mean of the 1000 runs at each energy, and a simplified code that would  
 180 calculate the proton energy loss along a straight line path through the tubs  
 181 and hodoscopes with small steps, using the proton stopping power and range  
 182 tables (PSTAR) from the National Institute of Standards and Technology  
 183 (NIST). The WbLS was modeled as water, and the LS as toluene.

184 The resulting energy depositions are listed in Table 1. The difference  
 185 between the two methods is taken as the uncertainty for the values obtained  
 186 (summed as square root of the sum of the squares with the RMS of the

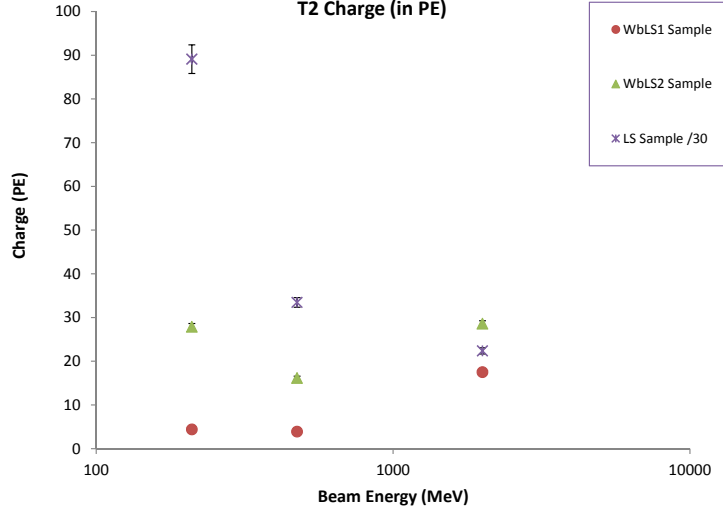


Figure 9: The light yield in PE for T2.

mean). The converted into the PE/MeV light yield is shown in Figure 10 for the T1 and in Figure 11 for the T2.

We see that the PE/MeV light yield is the same for LS at proton energies of 2GeV and 475MeV on both tubs, indicating that the Cerenkov light contribution is negligible for LS. It is not so for the WbLS, there is a significant LY change between these two energies. However, at 475MeV, there is virtually no Cerenkov light contribution to the total LY, thus, can use the data at this energy for LS to WbLS comparison and for obtaining the LY of the scintillator components of the WbLS. Figure 12 and Figure 13 show the ratio of the WbLS signal to the LS signal for the T1 and T2 at the proton energy of 475MeV, and the same ratio for the T2 only for the 210MeV (due to the saturation of the LS signal in T1 at this energy).

### 3.7. Light Yield in Photons/MeV

An estimate of the LY in photons/MeV is also possible. The calibration needed here is to estimate the efficiency if the PMT readout from the T1 and T2. Typically, this is a difficult task to carry out exactly, so two simple methods have been used to do this estimate.

First method is based on the fact that the LY is photons is known for the LS to be 10k photons/MeV for a MIP signal [5]. Since the proton at

Table 1: Energy Deposition in Samples

Beam Energy (MeV)	Sample	T1 Energy Deposit (MeV)	T2 Energy Deposit (MeV)
210	Water, WbLS	72.7±3.1	107.5±6.1
	LS	59±	124±
475	Water, WbLS	40.4±2.0	43.7±2.2
	LS	34±	36±
2000	Water, WbLS	28.6±2.6	28.7±3.1
	LS	24±	24±

206 2GeV has the same dE/dx as MIP, this dataset can be used to get the  
 207 approximate efficiency for each tub (e.g. PE to photon conversion) and use  
 208 it for the WbLS data. The second one can be used for T1 only and it was  
 209 used to check the validity of the first method. The difference between the  
 210 methods was added to the total uncertainty of the result. For T1, we can  
 211 use the 2GeV proton data on water to try and estimate the number of the  
 212 protons produced using the Equation 1 that is commonly used to estimate  
 213 the photon LY for the Cerenkov radiation in water [need reference or no/].

$$\frac{dN}{dx} \approx 370z^2(E_{max} - E_{min} - \frac{1}{\beta^2} \frac{E_{max} - E_{min}}{n_{ave}^2}) \quad (1)$$

214 The average index of refraction for the optical range was used, the  $E_{max}$   
 215 and  $E_{min}$  have been taken from the PMT sensitivity data. To get a better  
 216 estimate, the sensitivity range for the T1 PMT was divided into a number  
 217 of small sub-ranges with constant sensitivity and the results were weighted  
 218 by the sensitivity and combined together for a better estimate. Using the  
 219 resulting PE to photon conversion, the 2GeV proton LS data was used to  
 220 compare the number produced by the second method to the value used in  
 221 the first method. The result came very close to be 9713 photons/MeV for the  
 222 LS using the second method for T1.

223 The estimate results for the WbLS data are presented in Figure 14 and  
 224 in Figure 15 for the T1 and T2 respectively. As it can be seen from these  
 225 figures, the estimate shows that the goal of about 100 photons/MeV has been  
 226 reached using the WbLS2 sample, and different LY are possible by adjusting

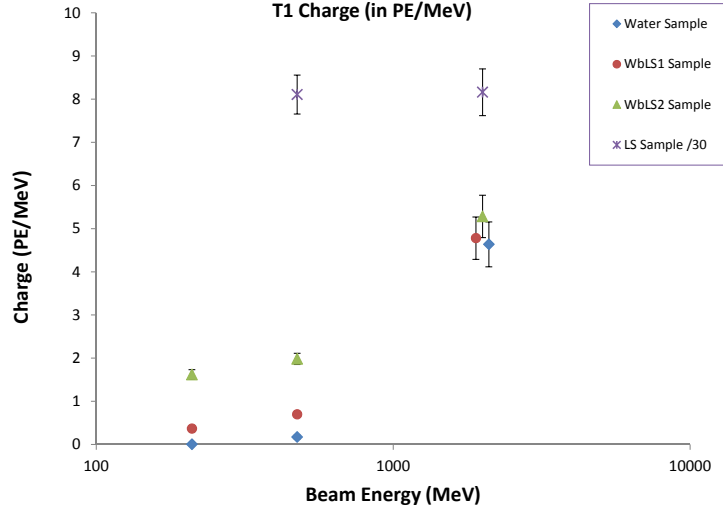


Figure 10: The light yield in PE/MeV for T1. At 2GeV beam energy, some points are offset for clarity.

the concentrations.

### 3.8. Systematics

A number of the systematic effects have been identified. Their effects have been accounted for in all the results presented.

During the experiment, the tubs with samples had to be disconnected and samples changed. An effect on the PMT of turning biasing on and off and exposing the PMT to ambient light during the disconnects. There is some minor variation in PMT noise and gain for less than 2 minutes after bias is turned on before a steady state is reached. Typically, there was at least a 5 to 10-minute interval between the installing the new sample in the beamline and data taking (the time was needed for the beam tuning process) thus greatly diminishing the influence of this effect on the data. In addition, there was very small variation in gain between each steady state; this variation has been added into the single PE calibration uncertainty.

A long-term stability of the single PE calibration was studied after the data taking for the 450 hours. The LED calibration was collected over 2h periods and the resulting variation ( 1%) was added into the single PE calibration uncertainty.

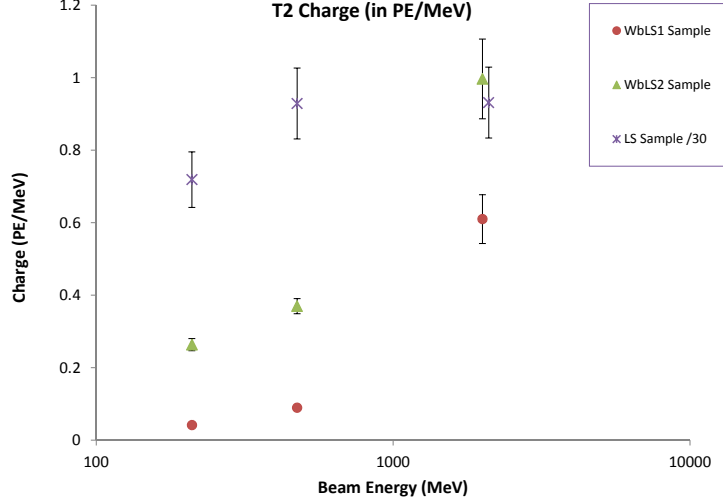


Figure 11: The light yield in PE/MeV for T2. At 2GeV beam energy, some points are offset for clarity.

245 The effects on the result due to the fitting procedure has been described  
 246 in subsection 3.5.

247 Another systematic effect arises from the window size selection process  
 248 during the waveform analysis described in subsection 3.2. The integration  
 249 window size had to be optimized to fit all signal widths from all the data  
 250 samples collected. If the window is too narrow then some signal may be  
 251 lost in the integration, if its too large - too much noise will be integrated  
 252 together with the signal and may add a non-zero contribution due to not all  
 253 noise being random. A comprehensive study was carried out to determine  
 254 the window size (300ns) and the effect of this choice on the fitted means for  
 255 each sample. The effect turned out to be small (the largest contribution of  
 256 this effect to one of the samples being less then 0.5%, smaller yet for all  
 257 others) and it is accounted for in the total fit uncertainty together with the  
 258 uncertainties estimated due to the fitting procedure.

## 259 4. Conclusion

260 in conclusion, we got the 100 photons/MeV, hooray... :):):)

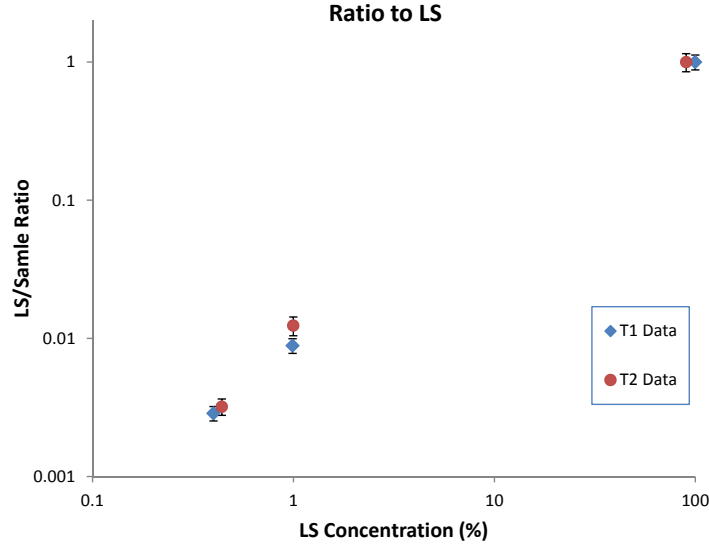


Figure 12: The WbLS light yield ratio to LS at 475MeV. Some points are offset for clarity.

## References

- [1] M. Fechner et.al. (The Super-Kamiokande Collaboration), ‘Kinematic reconstruction of atmospheric neutrino events in a large water Cherenkov detector with proton identification’, Phys. Rev. D 79 (2009) 112010, arXiv:0901.1645
- [2] Hamamatsu Photonics, 314-5 Shimokanzo, Toyooka-village, Iwatagun, Shizuoka-ken, 438-0193 Japan; <http://www.hamamatsu.com>
- [3] CAEN (Costruzioni Apparecchiature Elettroniche Nucleari S.p.A.), Via della Vetraria 11, 55049 Viareggio, Province of Lucca, Italy, 0584 388398.
- [4] Phillips Scientific, 31 Industrial Ave. Suite 1, Mahwah, N.J. 07430
- [5] C. Aberle, A. Elagin, H. J. Frisch, M. Wetstein, L. Winslow, ‘Measuring Directionality in Double-Beta Decay and Neutrino Interactions with Kiloton-Scale Scintillation Detectors’, arXiv:1307.5813 [physics.ins-det]

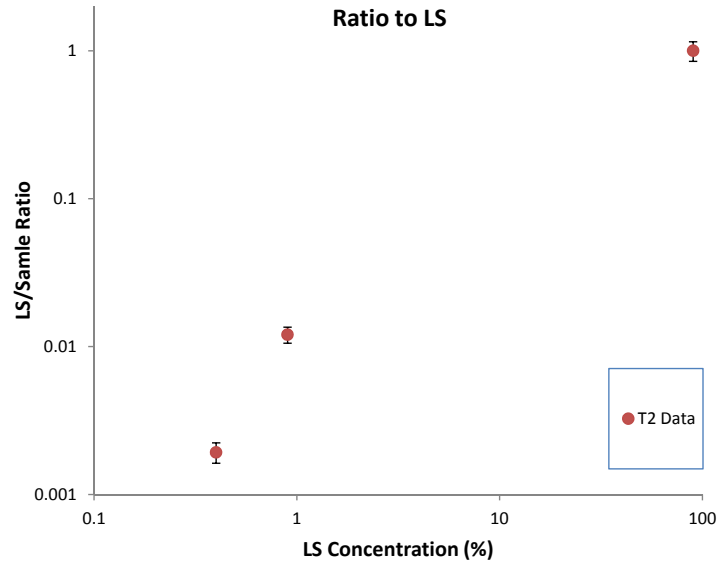


Figure 13: The WbLS light yield ratio to LS at 210MeV. Only data for T2 is shown.

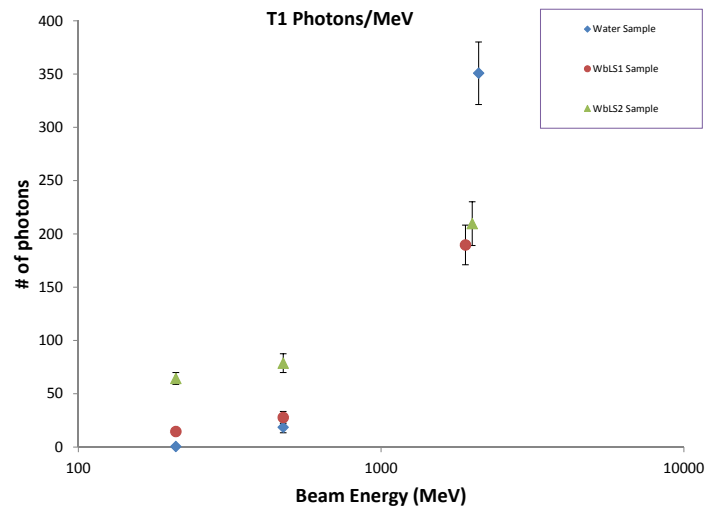


Figure 14: The light yield in Photons/MeV for T1. At 2GeV beam energy, some points are offset for clarity.



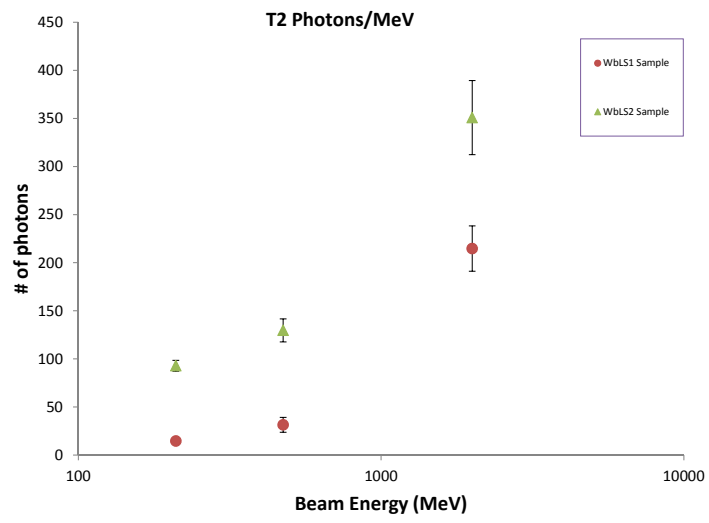


Figure 15: The light yield in Photons/MeV for T2.